AIAA JOURNAL
Vol. 39, No. 11, November 2001

Half Model Restrictions for Linear Plug Nozzle Testing

Menko E. N. Wisse* and Willem J. Bannink†
Delft University of Technology, 2629 HS Delft, The Netherlands

Linear plug nozzles have been receiving more attention since the development of the single stage to orbit reusable launch vehicle. To clarify the fundamental features of linear plug nozzle flow, experiments have been performed with half models because the design of the plug nozzle is symmetric. Experimental and numerical results are presented to investigate the usefulness of a half model design. The experiments were conducted on a half model without external flow and with an external flow at a Mach number of $M_\infty = 2$. The results have been used to validate computations using Navier–Stokes equations provided with a Baldwin–Lomax turbulence model and a Degani–Schiff correction. For comparison computations were performed for a full model subjected to the same conditions. For all of these conditions, the effects of increasing or decreasing pressure ratio have been taken into account.

Nomenclature

A	=	area
A^*	=	sonic area
C_D	=	drag coefficient
C_F	=	thrust coefficient
E	=	thrust coefficient error
F	=	thrust
L	=	full plug length
M	=	Mach number
p	=	pressure
T	=	temperature
X, Y, Z	=	coordinates
γ	=	ratio of specific heats
θ_t	=	tilt angle of the throat

Subscripts

c	=	chamber conditions
d	=	design conditions
e	=	exit
nb	=	nozzle base
nr	=	nozzle ramp
t	=	throat
t	=	stagnation conditions
vb	=	vehicle base
∞	=	freestream conditions

Introduction

THE key demands on future space transportation systems are the reduction of Earth-to-orbit launch costs in conjunction with an increase in launcher reliability and operational efficiency. A possible approach to provide cheaper access to space relies on the use of a single-stage-to-orbit (SSTO) reusable launch vehicle (RLV). Such an RLV will reduce the costs to get payload into space to $\frac{1}{10}$ of the original costs. One of the biggest challenges to achieve this is to develop a lightweight propulsion system that has an optimum performance during the entire launch trajectory. Therefore, a 40-year-old idea will enter the scene again, the linear aerospike engine or linear plug nozzle engine.

Plug nozzles possess beneficial properties that satisfy the requirements of minimizing vehicle weight and maximizing engine thrust.[1]

1) The altitude adaptation property gives the plug nozzle an important performance advantage with respect to a bell nozzle by self-adjusting the effective nozzle area ratio. At low altitudes (relatively high ambient pressures), the efficiency in thrust can be considerably higher than that of a bell nozzle.

2) A better utilization of the vehicle base is accomplished due to the following features. First, the plug nozzle reduces the harmful drag producing base area. Second, because almost the entire vehicle base can be utilized as nozzle exit area, very large nozzle area ratios may be obtained, which is to the benefit of a higher thrust performance in vacuum. Third, the thrust load is distributed over a large effective vehicle base area occupied by the plug, offering a possibility to reduce the weight of the thrust generating structure. In contrast, the bell nozzle is subject to a point source load.

However, plug nozzles should be studied in conjunction with the vehicle forebody because local external flow variations caused by the forebody affect the efficiency of the plug nozzle. The interaction between external flow and the expanding jet along the plug contour may change the beneficial concept of its altitude compensating capabilities. In subsonic flight, the jet will entrain the ambient flow, and in transonic and supersonic flight, the external flow over the vehicle expands into the vehicle base, region and induces a decrease in vehicle base pressure, causing the exhaust jet to overexpand, with a resultant dramatic degradation of the plug nozzle performance.

The present study concerns experiments and numerics on a linear plug nozzle placed in a supersonic external flow. Experimentally, surface pressures along the ramp, the nozzle base, the vehicle base, and downstream of the nozzle base were measured. The effects of plug truncation and increasing or decreasing pressure ratio (p_c/p_∞) were determined. Schlieren recordings of the flowfield were made. Numerically, the differences between a half model and a full model were determined.

Experimental Apparatus

The experiments have been performed in the supersonic wind tunnel ST-15 of the Department of Aerospace Engineering at the Delft University of Technology, a blowdown facility with fixed interchangeable nozzle blocks. Specially adapted liners were provided to serve as test setup for the present configuration.

The selected geometry is symmetric with respect to the wind-tunnel vertical symmetry plane; it uses the full width of the test section, 150 mm. $Y = 0$ is the middle of the test section. The model, shown in Fig. 1, has an overall height of 67.23 mm. The nozzle exit is sonic with a throat height of $A_t = 4$ mm, and the width of the nozzle throat is such that the entire test section width is covered. The tilt angle of the nozzle throat is $\theta_t = 67.84$ deg; it corresponds to the Prandtl–Meyer angle to deflect the flow to the horizontal direction resulting in the design Mach number of $M_d = 4.16$ and a design pressure ratio of $p_c/p_\infty = 188$. The corresponding ratio of exit area to throat area at design conditions is $A_d/A_t = 12.35$. The expansion is introduced by a nozzle lip at the upper end of the sonic nozzle exit. The vertical vehicle base of the forebody ends with its lower

Received 14 July 2000; revision received 7 February 2001; accepted for publication 30 April 2001.

*Research Fellow, Department of Aerospace Engineering, Kluyverweg 1.
†Associate Professor, Department of Aerospace Engineering, Kluyverweg 1.

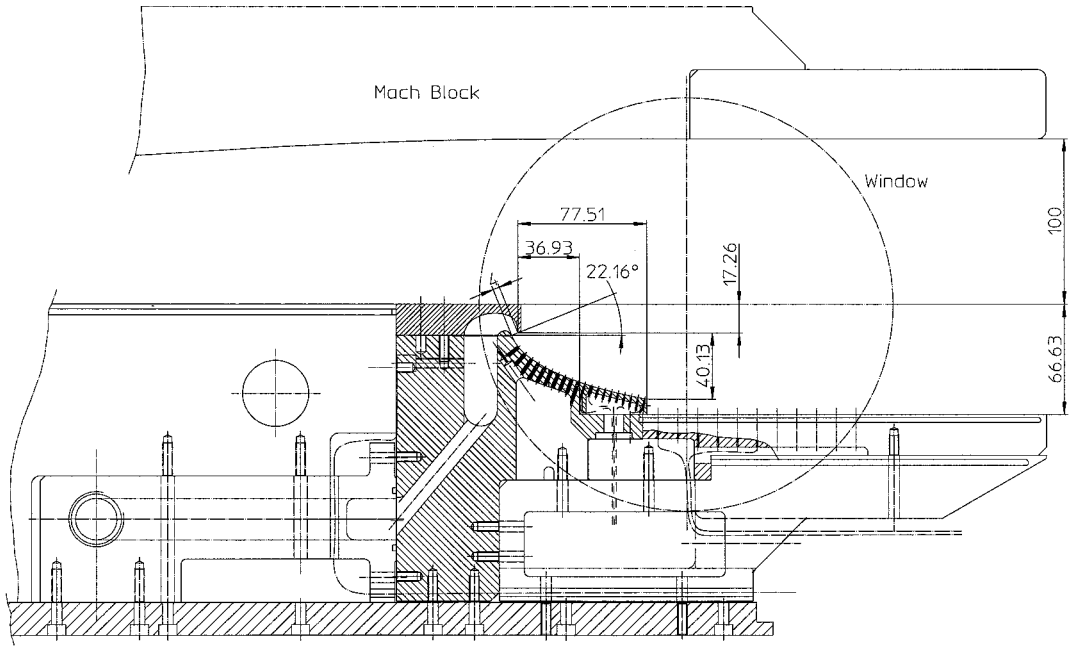

Fig. 1 Plug nozzle model showing some construction details.

part in the lip. The plug is a solid boundary following a streamline from a Prandtl–Meyer expansion (simple wave) starting at the sonic nozzle exit. Details on plug nozzle design are given in Ref. 2. A full plug, that is, from the starting point of the plug ramp (throat) to the lower tunnel wall, would have a plug length of $L = 203.2$ mm. Plug lengths truncated to 20 and 40% of the full plug length were used. Thus, the model consists of two bluff bases: a free vehicle base and a nozzle base.

Numerical Tools

Numerical simulations of the viscous (turbulent) flows over the 40% plug geometry were performed using a Navier–Stokes code developed at the Delft University of Technology.[3] The code is based on a cell-centered finite volume discretization. It is provided with second-order accurate upwind discretization according to the flux-vector splitting of Van Leer. Higher-order spatial discretizations are obtained with MUSCL, an interpolation technique with a Van Albada limiter to suppress spurious oscillations at discontinuities. The viscous terms are discretized using central differences.

The system of nonlinear discretized equations is solved with an implicit line-Gauss–Seidel method within an efficient nonlinear multigrid solution procedure. Within this multigrid, the solutions at the different grid levels have been smoothed by an implicit relaxation method.

For the calculations a Baldwin–Lomax turbulence model[4] was used with and without a Degani–Schiff correction.[5] The algebraic Baldwin–Lomax turbulence model[4] is accurate for steady flows with little or no separation; however, it is easy to use and economic. The Degani–Schiff correction[5] is capable of choosing the appropriate length scale for these separated flows. The turbulence generation process is dominated by the attached boundary layers, rather than the vortical flows. The Degani–Schiff correction defines this length scale and simulates, therefore, the eddy viscosity in base flow and the shock wave/boundary-layer interaction region more properly.

Plug Nozzle Flow Physics

Altitude Adaptation

The attractive feature of the plug nozzle mentioned in the Introduction is shown in Fig. 2. Hagemann et al.[6] divide the flow physics into three major categories. For pressure ratios lower than the design pressure ratio of a plug nozzle (Fig. 2a), the flow primarily expands along the central plug body to the ambient pressure p_∞. Only the first part of the nozzle ramp acts as an expansion contour down to the point where the last right running characteristic, which feels the ambient pressure, meets the ramp. When this characteristic is passed, the flow is adapted to the ambient pressure and is inclined toward the centerline. Downstream of this characteristic, the slope of the ramp, designed as clean expansion contour at its design pressure ratio, deviates the uniform flow outward, thereby generating compression waves that run toward the outer freestream shear layer. The interaction of the compression waves with the shear layer triggers a further expansion downstream. Finally, a system of recompression shocks and expansion waves adapts the exhaust flow to the ambient pressure. At the design pressure ratio (Fig. 2b), the straight characteristic with the design Mach number corresponds to a flow direction parallel to the centerline, and thus the shear layer is also parallel to the centerline. At pressure ratios above the design pressure ratio (overexpansion) (Fig. 2c), the pressure distribution along the plug ramp remains the same as for the design pressure ratio. In this way the expanding jet is not fully used for thrust.

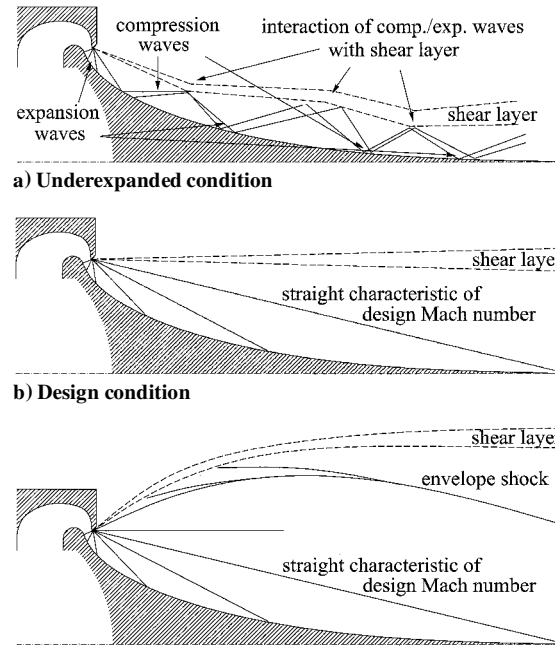

Fig. 2 Flow phenomena on a plug with full length at different pressure ratios p_c/p_∞.

This altitude adaptation is because the plug nozzle jet is not enclosed as in the case of a bell nozzle. Its gases are expanded in such a way that the jet is always exposed to the ambient pressure. As long as the pressure ratio is below the design value, compression waves in the jet impinge on the plug ramp generating high static pressures through recompression mentioned earlier. The plug nozzle loses its capability for further altitude adaptation beyond its design condition.

Plug Truncation

More than half of the full length plug produces almost no thrust and adds only weight to the system. From that point of view it may be removed leaving a truncated plug. It results in a different flow and performance behavior as compared to the full-length plug.[6] At lower pressure ratios, an open wake flow establishes (Fig. 3a). At a certain pressure ratio close to the design pressure ratio of the full length plug nozzle, the base flow reaches the closed form, characterized by a constant ratio of nozzle base pressure p_{nb}/p_c that is no longer influenced by the ambient pressure (Fig. 3b). This is the pressure ratio where the last right running characteristic has traveled beyond the base flow region. For this pressure ratio and higher pressure ratios, the pressure p_{nb}/p_c within the closed wake remains constant (Fig. 3c).

Base Flow

Although base flow is a well-known flow phenomenon and has been studied and analyzed for many years, reliable prediction of base drag is still beyond the reach of modern numerical simulation. A qualitative treatment of the base flow is given subsequently. Assume the two-dimensional flow generated in the vicinity of the base of a flat surface placed in a uniform supersonic flow. Figure 4 shows the schematic features of this flow pattern in a numerical plot. The flow is divided into three major components[7]: 1) an inviscid flow region, 2) a dissipative mixing layer, and 3) a base region.

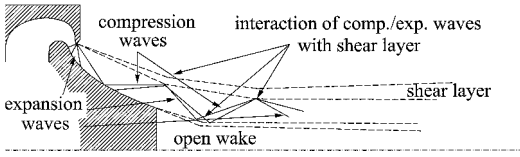

a) Underexpanded condition

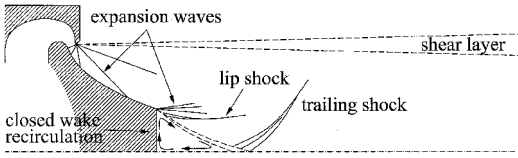

b) Design condition

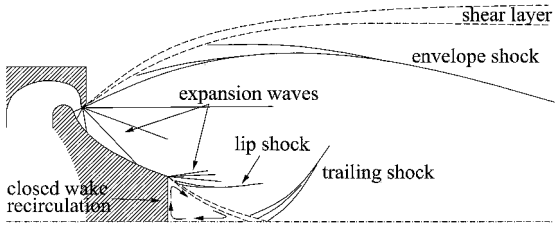

c) Overexpanded condition

Fig. 3 Flow phenomena of a truncated plug at different pressure ratios p_c/p_∞.

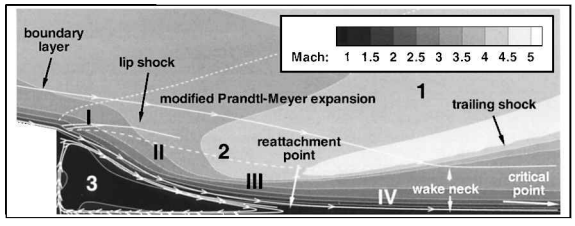

Fig. 4 Numerical Mach plot showing the schematic features in the flow pattern behind the nozzle base.

Because the base pressure is less than the pressure in the approaching flow, the viscous boundary layer of the flat plate expands around the sharp edge, forming a free shear layer. The corner expansion process (I; Fig. 4) is a modified Prandtl–Meyer pattern distorted by the presence of the approaching boundary layer. A Stokes-like flowfield in the immediate vicinity of the corner allows the flow to expand to a pressure lower than the base pressure. As the flow breaks away from the base plane, it is brought back to the base pressure by a weak compression shock, known as the lip shock. This phenomenon is described in more detail in Ref. 8. Downstream of this shock, the free shear layer begins to form. Entropy gradients are generated in this phase (for instance, across the shock and across the slip line, dividing the base and external flow; see Fig. 4), which leads to the production of vorticity and a recirculating flow.

The entropy produced across the lip shock and across the slip line will be partially diffused by viscous effects acting in the dissipative mixing layer (II; Fig. 4) until a final configuration is reached, with equilibrium between production of entropy within the region and its diffusion in the external main flow. The shear layer is turned back by means of a first compression fan (III; Fig. 4) spreading from the $M = 1$ contour into the freestream until the reattachment point is reached. Further compression (IV; Fig. 4) takes place forming the wake neck. The recompression waves coalesce to form the trailing shock. As the mixing layer or shear flow approaches this high-pressure region, it is decelerated accordingly. In fact, it will decelerate or be diffused until the static pressure in the shear flow equals that behind the recompression zone. The type of velocity profile in the shear layer just before the recompression zone indicates that a significant portion of this layer has a relatively low velocity or kinetic energy. This portion of the shear layer has insufficient kinetic energy to penetrate this recompression region and is recirculated back into the base region.

According to the Crocco–Lees theory,[9] a singular point with saddle behavior has been formed in the second compression region (IV; Fig. 4). This critical point, where $M = 1$, acts in the same way as a converging–diverging channel. It provides, therefore, a unique solution for the base pressure.

External Flow Effects

The aspect of external flow effects will now be taken into account. The conditions at transonic and low supersonic external flow will be considered because of its dramatic influence on the decrease in thrust performance. This performance loss is primarily caused by the local flow phenomena in the vehicle base region around the vehicle aft end.[1]

The external freestream expands around the vehicle base to a pressure p_{vb}, which is much lower than the external flow pressure. Initially, the exhaust jet overexpands to this low pressure and moves outward. Farther downstream, where the ambient pressure is higher, the jet is turned inward. Inside the jet, this generates compression waves, which coalesce into the envelope shock. The shock eventually impinges on the plug ramp (Fig. 5a) or downstream of the plug base. For high pressure ratios p_c/p_∞, the envelope shock may have passed the subsonic region of the wake (Fig. 5b). Then the base flow is insensitive to the ambient pressure (closed wake).

Experiment Description

Measurements were performed at a freestream Mach number of $M_\infty = 2$ with increasing pressure ratio p_c/p_∞, at a wind-tunnel stagnation pressure of $p_{t_\infty} = 4.1$ bar and a chamber and wind-tunnel stagnation temperature of $T_t = 278$ K. Measurements were also performed without an external flow. In that case, the jet operated as an ejector, decreasing the initial surrounding pressure below the atmospheric value of 1.0 bar. Two series of measurements were made: one with a plug length of 20% and one with a plug length of 40%, both referenced to the full plug length. The jet stagnation pressure was varied between 1 and 20 bar, approximately. The tunnel is not capable of achieving the design pressure ratio of $p_c/p_\infty = 188$. The tested conditions were, therefore, highly underexpanded. Starting

Table 1 Test matrix of experiments using schlieren video recordings

M_∞	Plug, %	p_{t_∞}, bar	p_c, bar	p_c/p_∞
0	20	1.0–0.7	1.4–16.7	1.4–25.7
0	40	1.0–0.6	1.9–18.5	1.9–31.8
2.0	20	4.1	1.3–15.1	2.5–28.8
2.0	40	4.1	1.8–16.1	3.5–31.2

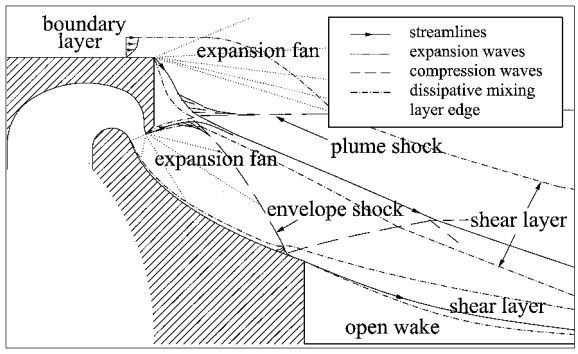

a) Open wake

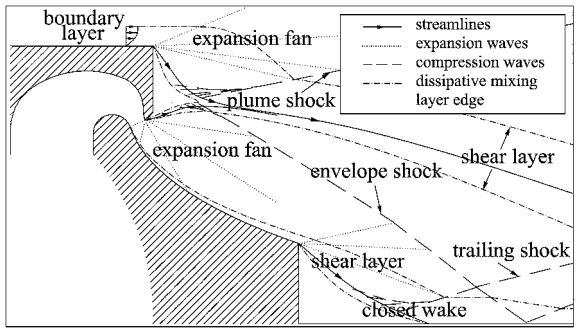

b) Closed wake

Fig. 5 Flow phenomena with supersonic external flow.

at a low jet stagnation pressure, the pressure is increased during a run with a step interval of about 0.5–1.0 bar. The test matrix is given in Table 1. The flow is visualized by means of schlieren video recordings.

The wind-tunnel flow conditions are accurate within ±0.5% in wind-tunnel stagnation pressure p_{t_∞}, within ±0.9% in chamber stagnation pressure p_c, and within ±3 K in stagnation temperature of the wind-tunnel flow and of the jet T_t.

Description of Computations

The 40% plug nozzle geometry was used for the numerical calculations. The flow is assumed to be two dimensional. The corresponding grid, shown in Fig. 6, consists of 44,890 cells. Grid convergence (Fig. 7) has been proven by means of a comparison between calculations with this refined grid, with a course grid consisting of 4,435 cells, and with a medium grid consisting of 14,514 cells for a freestream Mach number of $M_\infty = 2$ and a pressure ratio of $p_c/p_\infty = 31.2$. The resulting drag coefficient of the entire nozzle C_D differed between the course grid and the medium grid 2.6% and between the medium grid and the refined grid only 0.036%. Also further enlargement of the lower tunnel wall did not produce significant variation in the results. Therefore, the number of grid points were found to be sufficient for the remainder of the cases studied. To simulate the boundary layer of the external flow, a Blasius profile for compressible flow was imposed on the inflow plane. In the wind tunnel, the lower tunnel wall downstream of the half model may be considered as a no-slip wall. The effect on the flow characteristics of having a full model was simulated by means of a symmetry plane.

Calculations for each geometry have been performed at $M_\infty = 2$, $T_t = 278$ K, and $p_{t_\infty} = 4.10$ bar. In several cases it was very important whether the pressure ratio was increasing or decreasing. Therefore, calculations were started from results that would physically occur previously in time.

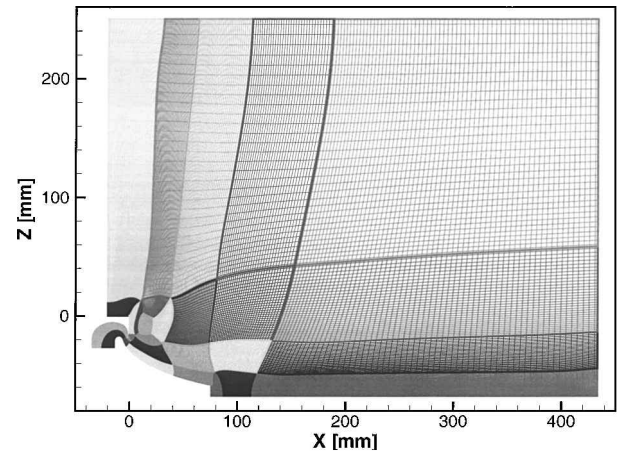

Fig. 6 Grid geometry.

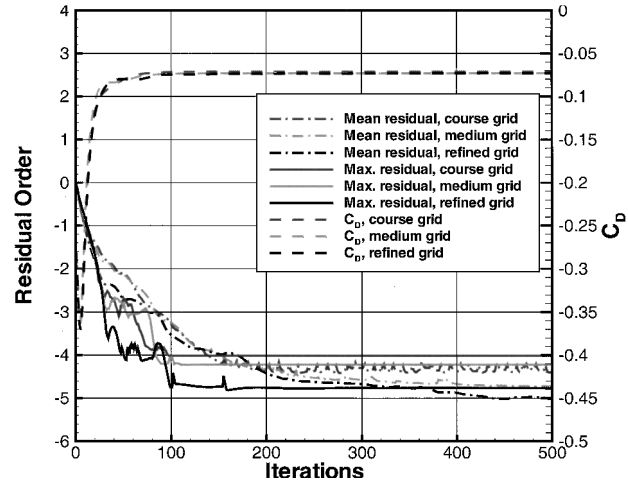

Fig. 7 Grid convergence of a course and a refined grid with p_c/p_∞ = 31.2 and M_∞ = 2.

To validate the numerical calculations with the experiments, calculations of the original 40% half and full model were performed for pressure ratios varying from $p_c/p_\infty = 3.50$ to 500.00. These turbulent Navier–Stokes calculations have been performed with a Baldwin–Lomax turbulence closure model[4] with and without a Degani–Schiff correction.[5]

Experimental Results

Vehicle Base Pressure Measurements

Vehicle base pressures have been measured for the 20% model without external flow and for both the 20% model and the 40% model with a $M_\infty = 2$ external flow. The results for the 20% model case without external flow are presented in Fig. 8a, which shows that the vehicle base pressure p_{vb} is almost equal to p_∞. Especially in the low range pressure ratios (p_c/p_∞), the vehicle base pressure is very much the same as p_∞. When the jet stagnation pressure p_c, is increased, the jet starts to operate as an ejector, decreasing p_∞. Actually, a low subsonic external flow is generated in this way. From the position where p_∞ was measured to the vehicle base, the channel is diverging. For a subsonic flow this means that the Mach number decreases and the static pressure increases. Therefore, the vehicle base pressure becomes higher than the measured p_∞.

The results for both the 40% model and the 20% model with a $M_\infty = 2$ external flow are presented in Fig. 8b. From Fig. 8b the conclusion may be drawn that, as may be expected, the vehicle base pressure depends strongly on the shock wave pattern, created by the interaction between the external flow and the jet. The difference between the two models is the length of the plug and, therefore, the plug base flow pattern. These patterns develop different Prandtl–Meyer expansions and trailing shocks. This phenomenon influences the

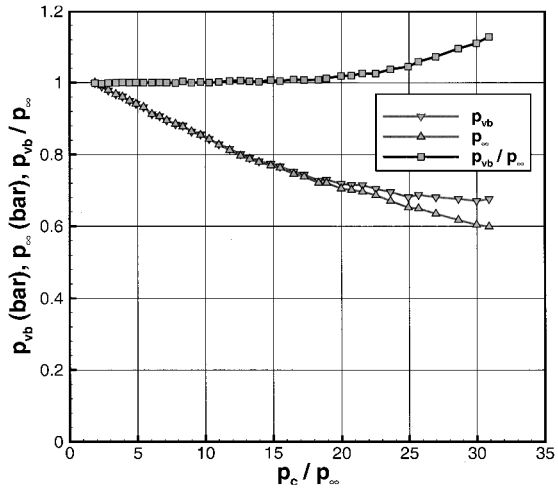

a) 20% model, $M_\infty = 0$

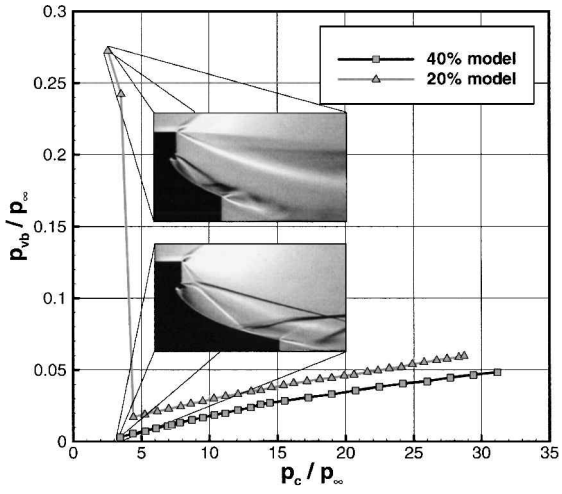

b) $M_\infty = 2$

Fig. 8 Vehicle base pressure measurements vs pressure ratio.

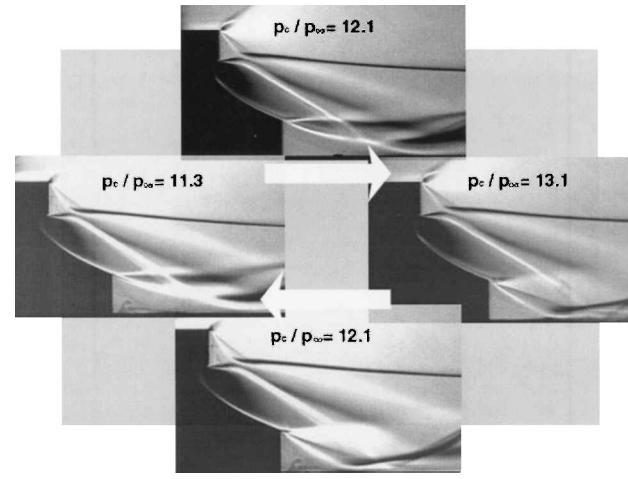

a) Nozzle base hysteresis schematics

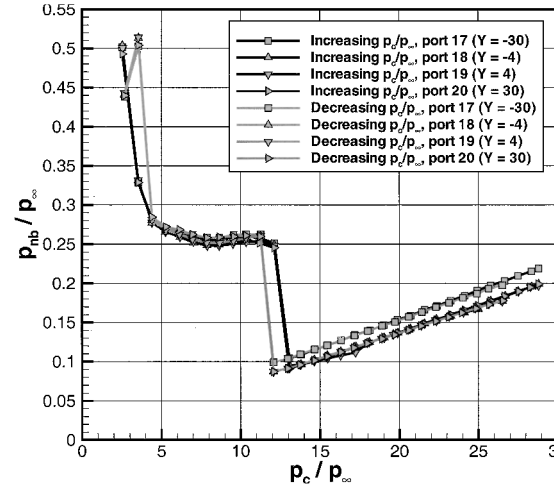

b) Nozzle base pressure measurements vs pressure ratio

Fig. 9 Nozzle base hysteresis: 20% model, $M_\infty = 2$, $X = 75.64$ mm, and $Z = -61.99$ mm.

entire shock wave pattern and, therefore, the vehicle base static pressure. For high-pressure ratios, the trend for both models is the same. The measured pressures of the 20% model are only slightly higher. However, large differences exist for low-pressure ratios. For the lowest pressure ratios of the 20% model, the vehicle base retains even its open wake (Fig. 8b), and the pressure in the vehicle base is, therefore, relatively high.

Nozzle Base Hysteresis

The present tests were made with increasing pressure ratio, and the closing of the wake for the 20% model with a $M_\infty = 2$ external flow occurred between pressure ratios $p_c/p_\infty = 12.1$ and 13.1. However, for a decreasing pressure ratio, the opening of the wake occurred between pressure ratios $p_c/p_\infty = 11.3$ and 12.1 (Ref. 10). This nozzle base hysteresis phenomenon can be explained by inspecting Fig. 9a. In Fig. 9a, the hysteresis is shown by means of schlieren pictures. In the case of the increasing pressure ratio, the base region is initially open. As long as the envelope shock impinges on the ramp or the recirculation region, the wake remains open. As soon as the shock passes the recirculation region, the wake closes. The recirculation region of a closed wake is much smaller than that of an open wake. Therefore, if the pressure ratio is decreased after the closing of the wake the envelope shock has to pass a larger distance before reaching the recirculation region again. The pressure drop and rise are plotted in Fig. 9b. For the 40% model, this phenomenon was not found. However, this does not mean that there is no nozzle base hysteresis present. Because of the smaller nozzle base and its location farther downstream, the hysteresis would appear in a smaller pressure ratio range. With the step sizes used in the experiments, this phenomenon could, therefore, not be captured.

Generated Thrust

The contribution of all of the parts of the plug nozzle to the total thrust are compared to that of an ideal, variable geometry nozzle and to a fixed nozzle with $M_d = 4.16$ ($p_c/p_\infty = 188$). The thrust coefficient C_F is defined as the ratio of thrust over the jet stagnation pressure p_c acting on the sonic throat area A^* (Ref. 1):

$$C_F = F/p_c A^* \tag{1}$$

For an ideal nozzle with fixed geometry, it is given by the following equation:

$$C_{F_{\text{fixed}}} = \gamma M_d \sqrt{\left(\frac{2}{\gamma+1}\right)^{(\gamma+1)/(\gamma-1)} \frac{1}{1+[(\gamma-1)/2]M_d^2}} + \frac{A_d}{A^*}\left\{\frac{1}{(1+[(\gamma-1)/2]M_d^2)^{\gamma/(\gamma-1)}} - \frac{p_\infty}{p_c}\right\} \tag{2}$$

For the ideal nozzle with variable geometry, the thrust coefficient equation becomes

$$C_{F_{\text{variable}}} = \gamma M_e \sqrt{\left(\frac{2}{\gamma+1}\right)^{(\gamma+1)/(\gamma-1)} \frac{1}{1+[(\gamma-1)/2]M_e^2}} \tag{3}$$

The thrust coefficient for the plug nozzle can be divided into parts. The contribution of the nozzle throat is the thrust due to the subsonic part of the nozzle:

$$C_{F_t} = \cos\theta_t\{2[2/(\gamma+1)]^{1/(\gamma-1)} - (p_\infty/p_c)\} \tag{4}$$

The contribution of the 0–20% ramp and 20–40% ramp has been calculated by a discretized integration of the static pressure measurements along the ramp:

$$C_{F_{\mathrm{nr}}} = \frac{1}{A^*}\int^{\mathrm{nr}} \frac{p - p_\infty}{p_c}\,\mathrm{d}z \tag{5}$$

The contribution of the nozzle base and vehicle base has been calculated with, respectively,

$$C_{F_{\mathrm{nb}}} = 1/A^*[(p_{\mathrm{nb}} - p_\infty)/p_c]\,h_{\mathrm{nb}} \tag{6}$$

$$C_{F_{\mathrm{vb}}} = 1/A^*[(p_{\mathrm{vb}} - p_\infty)/p_c]\,h_{\mathrm{vb}} \tag{7}$$

The resulting total thrust coefficient for the plug nozzle can then be calculated with

$$C_{F_{\mathrm{plug}}} = C_{F_t} + C_{F_{\mathrm{nr}}} + C_{F_{\mathrm{nb}}} + C_{F_{\mathrm{vb}}} \tag{8}$$

The performance of the 40% model with $M_\infty = 2$ external flow is shown in Fig. 10a. The overexpansion of the jet into the vehicle base causes the entire flow to deliver dramatic performance losses. The static pressure in the vehicle base produces in itself a very large drag. The low pressure at the vehicle base causes the jet flow to overexpand. The pressures on the ramp are, therefore, expanded to very low values, in particular for the low-pressure ratios. The nozzle base pressure is dependent on flow characteristics at the end of the ramp. The performance of the nozzle base is, therefore, dramatically deteriorated. Actually, the entire performance of both the 20 and the 40% model with an $M_\infty = 2$ external flow is deteriorated, as can also be seen in Fig. 10b. Note that, for high-pressure ratios, the performance losses are decreased. Therefore, assuming the chamber pressure of a real engine is $p_c = \pm 100$ bar, the pressure ratio would be always higher than $p_c/p_\infty = 100$.

The performance losses can be attributed to the generic shape of the vehicle base. Boattailing of this base would increase the performance substantially. Another improvement would be replacing the sonic inflow by a supersonic primary nozzle, whereby the throat angle can be reduced, and, therefore, the vehicle base size and the boattail angle. On the other hand, one can increase the design pressure ratio leaving the throat angle the same. This would retain the altitude adaptive capabilities for higher pressure ratios. For maximizing performance, this means that the pressure ratio over the supersonic primary nozzle should be as high as possible. When this primary nozzle is retained always overexpanded, this must be equal to the minimum pressure ratio during launch.

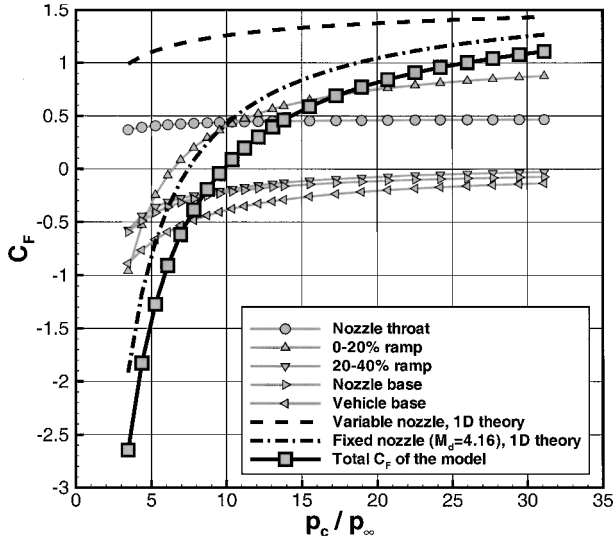

a) Contribution of the 40% plug parts

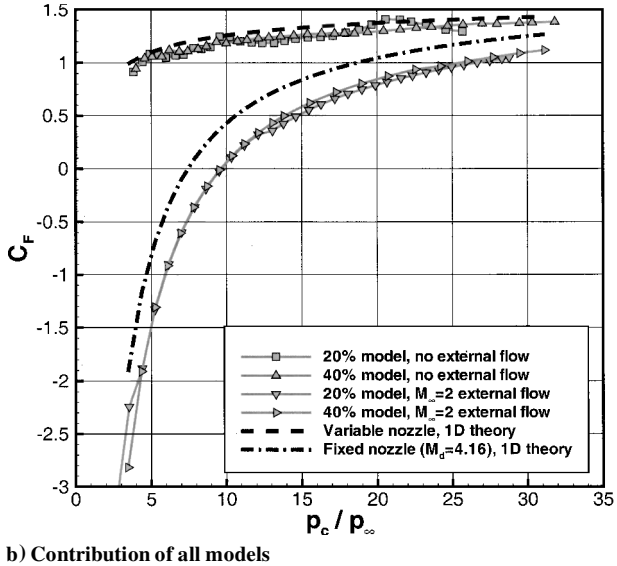

b) Contribution of all models

Fig. 10 Experimental thrust coefficient vs pressure ratio.

Validation of Numerics

For further computational analyses, the 40% plug model with $M_\infty = 2$ has been used. For this purpose the numerical method has been validated with the experimental results. The qualitative comparison of the experimental and the numerical results is quite good as can be seen in Fig. 11. The results shown in Figs. 11a–11c are obtained using the Baldwin–Lomax turbulence model[4] with Degani–Schiff correction.[5] For these conditions the Degani–Schiff correction gave the best results. The position of the shock waves is almost the same as for the experiments, although the Degani–Schiff correction underestimates the eddy viscosity, resulting in a larger separation bubble and in stronger reflected waves than in experiment. From $p_c/p_\infty = 24.2$ (Fig. 11d) to higher pressure ratios, the standard Baldwin–Lomax method[4] seems to give slightly better results.

The numerical treatment of the shock wave/boundary-layer interaction proved to be very difficult; see Fig. 12. This phenomenon shows a direct influence on the nozzle base performance. The resulting nozzle base pressures using the Baldwin–Lomax turbulence model[4] with and without Degani–Schiff correction[5] are taken at the same point as the pressure tabs during the experiments and are shown in Fig. 13. The standard Baldwin–Lomax model[4] is not capable of achieving the experimentally shown relatively high

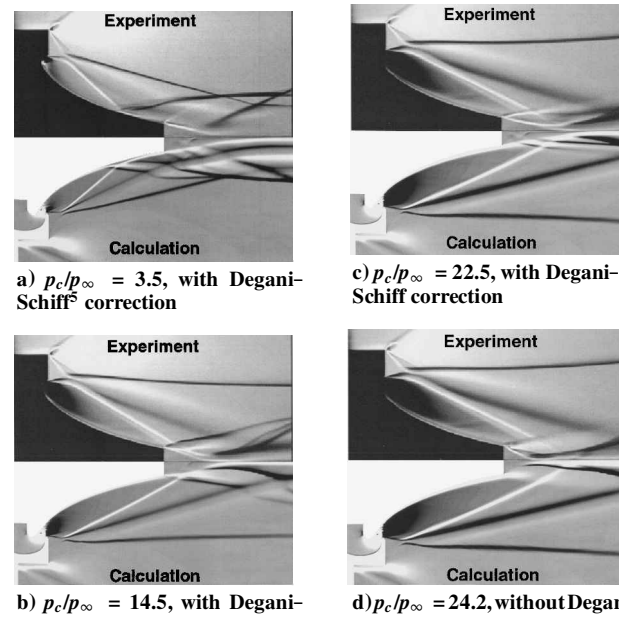

a) p_c/p_∞ = 3.5, with Degani–Schiff[5] correction

c) p_c/p_∞ = 22.5, with Degani–Schiff correction

b) p_c/p_∞ = 14.5, with Degani–Schiff correction

d) p_c/p_∞ = 24.2, without Degani–Schiff correction

Fig. 11 Numerical and experimental schlieren images of the 40% plug with M_∞ = 2.

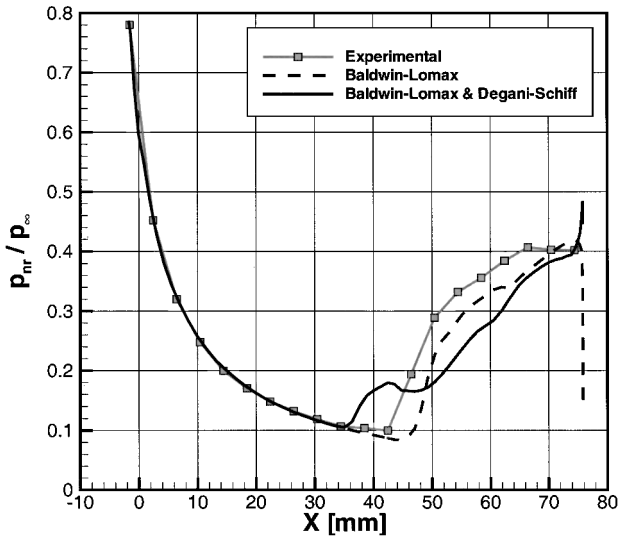

Fig. 12 Ramp pressure distribution of the 40% plug; $p_c/p_\infty = 3.5$ and $M_\infty = 2$.

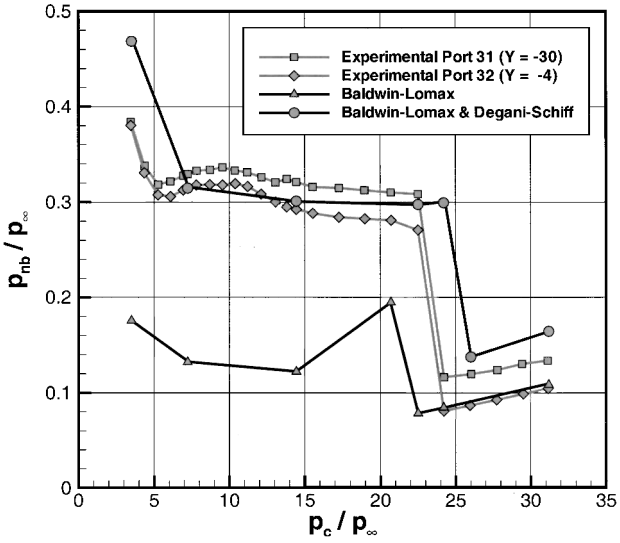

Fig. 13 Nozzle base pressure vs pressure ratio of the 40% plug nozzle; $M_\infty = 2$, $X = 75.64$ mm, and $Z = -61.99$ mm.

nozzle base pressures because of a poorly predicted boundary layer coming from the shock wave/boundary-layer interaction. However, for higher pressure ratios, the prediction of the nozzle base pressure seems to be even better than the prediction with the Degani–Schiff correction,[5] altough one has to keep in mind that the character of the nozzle base region is highly three dimensional. The Degani–Schiff correction overpredicts the eddy viscosity, which results in overpredicted nozzle base pressures in the closed wake regime. The transition from open to closed wake is, therefore, delayed from between $p_c/p_\infty = 22.5$ and $p_c/p_\infty = 24.2$ to between $p_c/p_\infty = 24.2$ and $p_c/p_\infty = 26.0$. The transition in the standard Baldwin–Lomax calculations[4] takes place at a much lower pressure ratio (between $p_c/p_\infty = 20.7$ and $p_c/p_\infty = 22.5$). The base pressure is underpredicted while the shock wave interacts with the ramp boundary layer or the shear layer. Therefore, the base region is much smaller, the transition occurs for lower base pressures, and the pressure drop is not as large as for the calculations with the Degani–Schiff correction.[5]

In Fig. 14 the vehicle base pressures from experiments and calculations are given. The calculated pressures are taken at the same point as the pressure tabs during the experiments. Figure 14 shows clearly that, in the cases where the envelope shock had altered the boundary layer, the numerical values of the vehicle base pressure p_{vb} were highly overpredicted. This could be caused by the poorly predicted shock wave/boundary-layer interaction on the ramp. The reflecting

Table 2 Quantification of thrust coefficients

p_c/p_∞	$C_{F_{Exp}}$	$C_{F_{BL}}$	$C_{F_{BLDS}}$	E_{BL}, %	E_{BLDS}, %
3.5	−2.6440	−2.8978	−2.7080	11.76	2.966
7.2	−0.5407	−0.6565	−0.5582	6.488	0.986
14.5	0.5084	0.4638	0.4904	2.670	1.075
22.5	0.9085	0.8753	0.8965	2.005	0.726
24.2	0.9577	0.9752	0.9732	1.059	0.941
31.2	1.1068	1.0920	1.1121	0.899	0.321

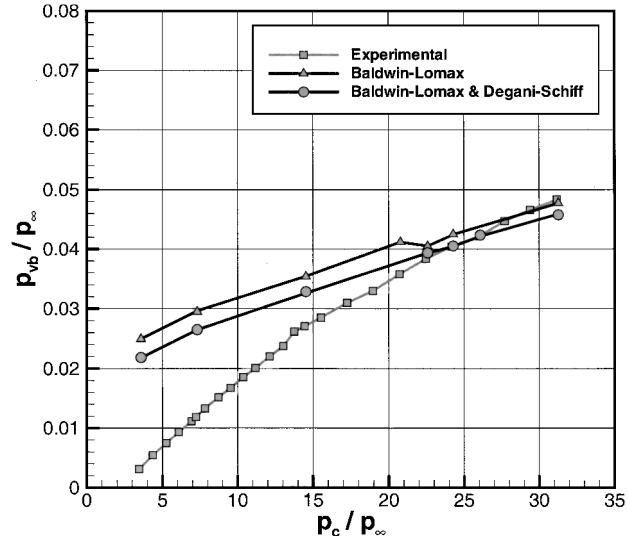

Fig. 14 Vehicle base pressure vs pressure ratio of the 40% plug nozzle; $M_\infty = 2$ and $Z = -3$ mm.

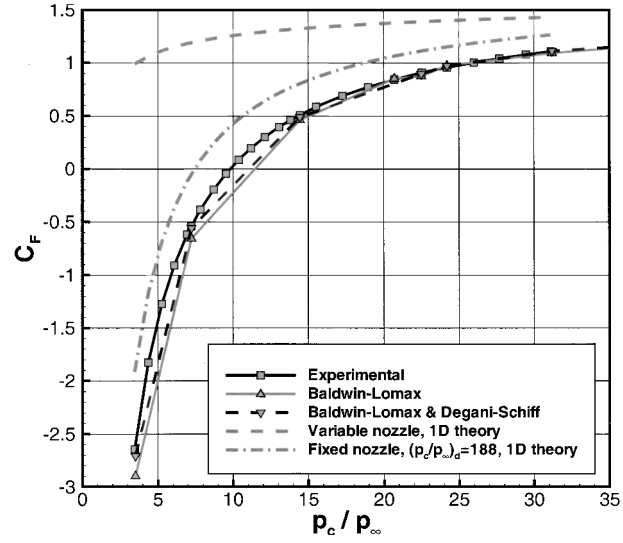

Fig. 15 Validation of thrust coefficient vs pressure ratio of the 40% plug nozzle; $M_\infty = 2$.

shock wave and boundary layer are, therefore, also incorrectly represented, and the entire flowfield is changed accordingly. Another factor of importance could be the instationary effects of the shock wave/boundary-layer interaction. This means that there are some differences concerning the base pressures. However, the computed thrust coefficients (Fig. 15) are quite similar with the experimental results because the results of the ramp pressure distribution are fairly good, and these are the most important for the thrust coefficient. The thrust coefficient error between the calculations and the test data have been quantified in Table 2, where the error is calculated by

$$E = \left| \frac{C_F - C_{F_{Exp}}}{C_{F_{Exp}} - C_{F_{No\,Thrust}}} \right| \tag{9}$$

Concluding, in the open wake regime with shock wave/boundary-layer interactions, the Degani–Schiff correction[5] shows the best results. For the more simple flow of the closed wake regime without such an interaction, the standard Baldwin–Lomax model[4] gives somewhat better results.

Half–Full Model Comparison

To find out whether the flow past a full plug nozzle model can be investigated in a wind tunnel by a half model, both situations have been simulated numerically for a 40% plug at $M_\infty = 2$. Because for the full model it appeared to be important whether the pressure ratios were increasing or decreasing, both have been shown separately. For the half model, the lower tunnel wall beyond the nozzle base was treated as a no-slip wall and for the full model as a symmetry plane. This distinction results in local differences in the nozzle base flow, which have large effects on the overall flow characteristics.

Vehicle Base Hysteresis

These large effects can be seen when increasing the pressure ratio from a solution with a subsonic jet flow. It was found that, unlike the half model, the full model keeps its vehicle base wake open during the low ranges of increasing pressure ratios. To trigger this phenomenon, calculations were started from pressure ratios for which the jet remained subsonic. In these cases the system of expansion and compression waves in the jet was capable of finding an equilibrium keeping the vehicle base wake open; see Fig. 16 ($p_c/p_\infty = 3.5$, top). Several recirculation regions are formed downstream of the nozzle base without being disturbed by a no-slip wall. The jet is separated from the symmetry plane and does not need a trailing shock anymore. This leads to an equilibrium with two separated supersonic flows: the jet and the external flow. For higher pressure ratios, the vehicle base pressure p_{vb} decreases, and the open vehicle base region becomes smaller; see Fig. 16 ($p_c/p_\infty = 7.2$, top). For a certain pressure ratio ($p_c/p_\infty = 14.5$), the shear layer of the exhaust jet and the external flow need to overlap each other to retain the open vehicle base. This is of course physically impossible, and the vehicle base closes itself. Decreasing the pressure ratio from this value causes the vehicle base to remain closed, until the jet is completely subsonic. This results in a vehicle base hysteresis phenomenon in between these pressure ratios. An open vehicle base wake could not be maintained in the case of the half model. In this case the subsonic nozzle base flow is decelerated by the no-slip wall. Feeding of these regions is more difficult, and the nozzle base pressure drops causing the jet to expand into the base. These expansion waves also impinge on the vehicle base recirculation regions. The pressure in these regions also drops, causing the exhaust jet at the throat and the external flow to expand further, too. The shear layers of these flows, therefore, touch each other, and finally expand further until a closed form of the vehicle base is formed.

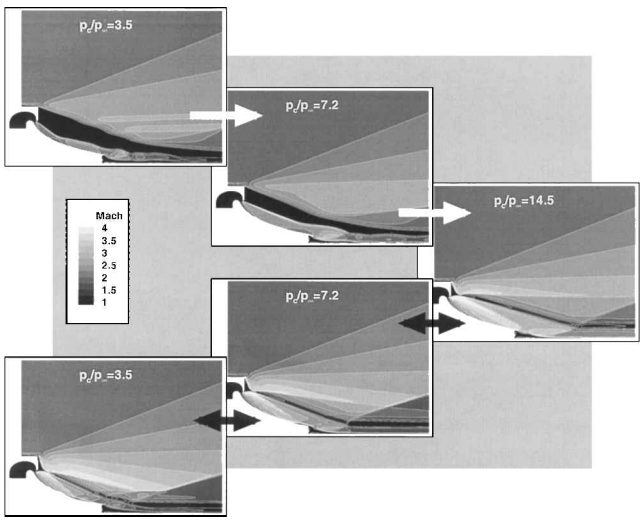

Fig. 16 Mach plot of vehicle base hysteresis; 40% plug nozzle, M_∞ = 2, Baldwin–Lomax[4] with Degain–Schiff correction.[5]

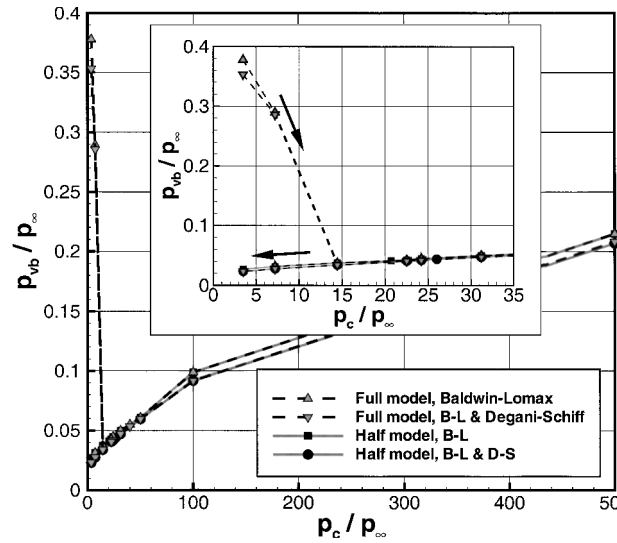

Fig. 17 Mean vehicle base pressure vs pressure ratio; 40% plug nozzle and M_∞ = 2.

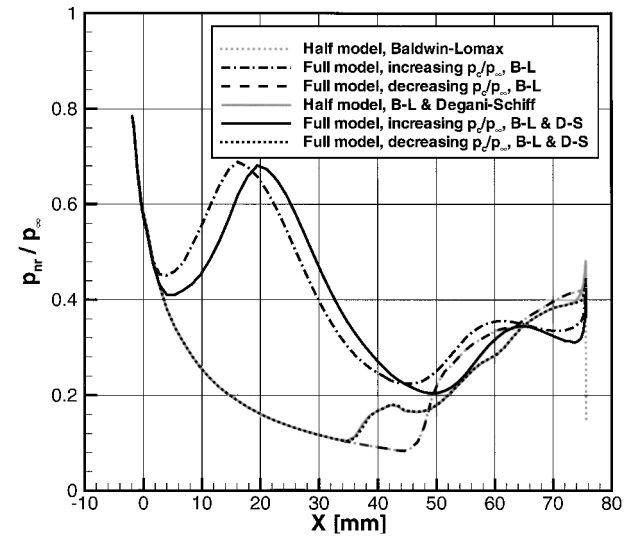

Fig. 18 Ramp surface pressure distribution; 40% plug nozzle, p_c/p_∞ = 3.5, and M_∞ = 2.

The open vehicle base wake causes the vehicle base pressures to be relatively high (Fig. 17). The pressure distribution along the plug ramp is, therefore, dramatically increased (Fig. 18). It appears that the differences between the half model and the full model pressure distributions for increasing and decreasing pressure ratio are significant, at least for these low-pressure ratios.

Closed Vehicle Base Wake

In case of a closed vehicle base wake, the full model has almost the same solutions as the half model. The differences are caused by the local flow phenomena downstream of the nozzle base.

The no-slip wall in the half model causes the viscosity to play a dominant part on the nozzle base flow (Fig. 19). The viscous layer on the lower wall triggers the development of larger secondary vortices. The pressure distribution in the vertical direction along the nozzle base is essentially flat for the half model cases because of the highly viscous energy exchanges in the entire base region. In the full model approximations, the lower wall, replaced by a symmetry plane, lacks the production of extra shear stress. Therefore, the turbulence intensity is much less, and large differences are present in the pressure distribution along the nozzle base (Fig. 19).

The mean pressure distribution along the nozzle base is also different. The dissipative mixing layer, which starts as a boundary layer before entering the base region, expands into the base region and becomes a free shear layer. Then it has to be turned axially by means of

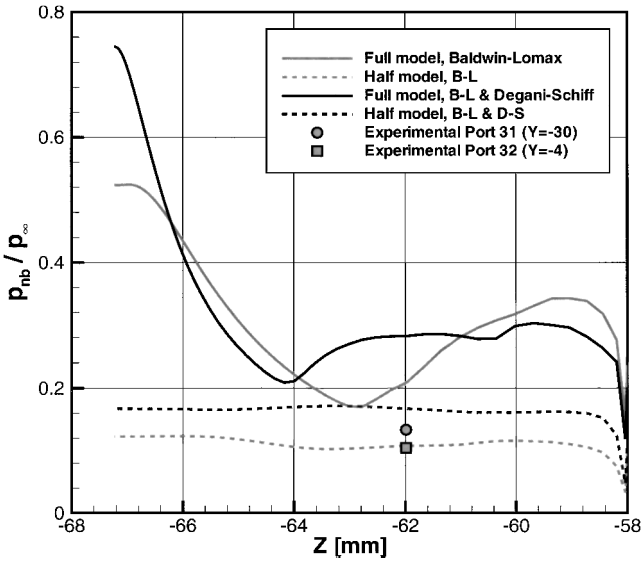

Fig. 19 Nozzle base pressure distribution; 40% plug nozzle, p_c/p_∞ = 31.2 and M_∞ = 2.

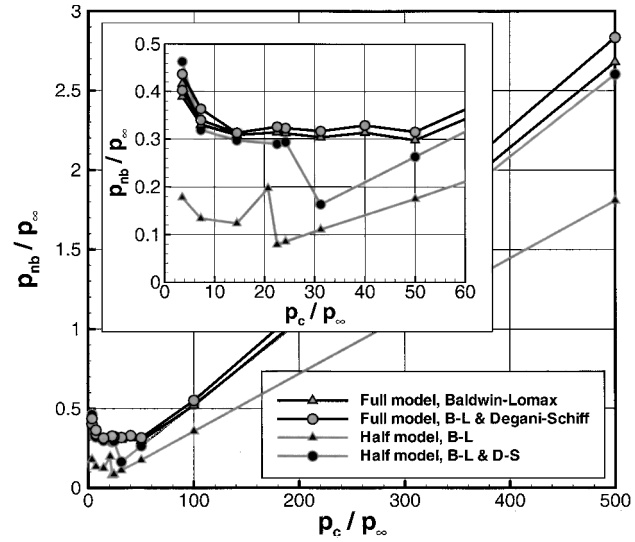

Fig. 20 Mean nozzle base pressure vs pressure ratio; 40% plug nozzle and M_∞ = 2.

compression waves, coalescing into the trailing shock, and creating the wake neck (Fig. 4). The wake neck velocity profile is dependent on the way the lower wall is prescribed. Just behind the reattachment point, where for the full model $M \approx 0$ also, the wake neck is larger than a half model's wake neck because of the symmetry conditions. The mean pressure at the nozzle base is, therefore, higher for a full model than for a half model (Fig. 20).

From Fig. 20 another difference between half and full model can be seen. Although for the half model a rapid pressure drop (wake closure) is shown between $p_c/p_\infty = 24.2$ and 26.0, the full model does not show such a rapid change in nozzle base pressure. This means that the influence of the envelope shock decreases gradually. In the case of the half model, the no-slip condition makes it harder for the recirculating flow to return from the reattachment point into the base region than in case of the full model. The full model does not encounter any wall shear stress, and the region will be much larger. Therefore, the envelope shock will influence the nozzle base pressure as in Fig. 21 until the envelope shock travels beyond the critical point ($M = 1$) of the base flow. At this pressure ratio, the influence of the shock is small, and no sharp drop can be seen.

The effect on the thrust coefficient of these differences are, however, of much less importance than the ramp pressure distribution, as can be seen from Fig. 22. The vehicle base hysteresis on the other hand shows much larger differences, which certainly cannot be neglected.

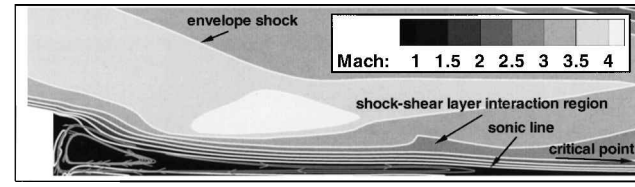

Fig. 21 Nozzle base Mach plot; 40% full model, Baldwin–Lomax[4] and Degani–Schiff correction,[5] p_c/p_∞ = 31.2, and M_∞ = 2.

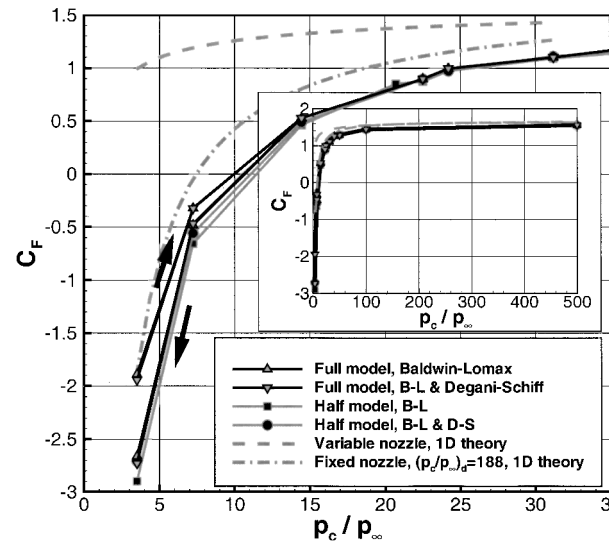

Fig. 22 Thrust coefficient vs pressure ratio; M_∞ = 2.

Conclusions

When comparing the experiments with increasing nozzle pressure ratio presented in this paper with the experiments with decreasing pressure ratio presented in Ref. 10, the conclusion may be drawn that there exists a nozzle base hysteresis. Because of the larger nozzle base area, the 20% model shows a larger base hysteresis region than the 40% model.

The validation of numerical tools have been performed with the Baldwin–Lomax turbulence model with and without the Degani–Schiff correction. In case of the low nozzle pressure ratio, where the envelope shock impinges on the ramp or on the nozzle base region (the open wake regime), the Baldwin–Lomax prediction of the boundary layer beyond the interaction is inaccurate, which results in nozzle base pressures that are too low. The Baldwin–Lomax model with the Degani–Schiff correction overpredicts the size of the shock wave/boundary layer interaction region, but simulates the boundary layer beyond the interaction quite well, resulting in good nozzle base pressure predictions. In the closed wake regime, the standard Baldwin–Lomax model gives somewhat better results.

The numerical comparison of the results between half and full model shows some interesting differences in flow topology. The local differences between both models influence the entire flow highly, especially for low-pressure ratios. A vehicle base hysteresis was found to be present in case of the full model, which could not be realized for the half model. The vehicle base wake remained open, when the pressure ratio was increased from a subsonic exhaust jet to supersonic values. When the shear layers from jet and external flow merge, the vehicle base wake closes. When the pressure ratio is decreased further from this condition, the vehicle base remains closed until the jet flow becomes subsonic. For higher pressure ratios, the local differences do not generate large differences in the rest of the flow. The differences are restricted to the local nozzle base flow quantities.

The pressure ratios involved in the vehicle base hysteresis are much lower than the real operational pressure ratios during launch. However, for different plug nozzle configurations the vehicle base hysteresis may hold for higher pressure ratios. On the other hand, for

boattailed configurations, where the external flow remains attached, no vehicle base hysteresis may exist at all. Then, keep in mind that the nozzle base flow quantities are different. Even then, one may conclude that a half model does not properly simulate a full model plug nozzle.

Acknowledgments

The authors would like to thank E. W. de Keizer, F. J. Donker Duyvis, and P. J. Duyndam for their technical and creative assistance throughout the experiments of this project.

References

[1]Ruf, J. H., and McConnaughey, P. K., "The Plume Physics Behind Aerospike Nozzle Altitude Compensation and Slipstream Effect," AIAA Paper 97-3218, July 1997.

[2]Angelino, G., "Approximate Method for Plug Nozzle Design," *AIAA Journal*, Vol. 2, No. 10, 1964, pp. 1834, 1835.

[3]van der Weide, E., Deconinck, H., Houtman, E. M., and Bakker, P. G., "Computational Analysis of Base Flow/Jet Plume Interaction," *Proceedings of the Third European Symposium on Aerothermodynamics for Space Vehicles*, SP-426-1999, ESA–European Space Research and Technology Center, Noordwijk, The Netherlands, 1999, pp. 605–612.

[4]Baldwin, B. S., and Lomax, H., "Thin Layer Approximation and Algebraic Model for Separated Turbulent Flows," AIAA Paper 78-0257, Jan. 1978.

[5]Degani, D., and Schiff, L. B., "Computation of Turbulent Supersonic Flows Around Pointed Bodies Having Crossflow Separation," *Journal of Computational Physics*, Vol. 66, No. 1, 1986, pp. 173–196.

[6]Hagemann, G., Immich, H., and Terhardt, M., "Flow Phenomena in Advanced Rocket Nozzles: The Plug Nozzle," AIAA Paper 98-3522, July 1998.

[7]Chapman, D. R., "An Analysis of Base Pressure at Supersonic Velocities and Comparison with Experiment," NACA TN 2137, July 1950.

[8]Weinbaum, S., "Rapid Expansion of a Supersonic Boundary Layer and Its Application to the Near Wake," *AIAA Journal*, Vol. 4, No. 2, 1966, pp. 217–226.

[9]Crocco, L., and Lees, L., "A Mixing Theory for the Interaction Between Dissipative Flows and Nearly Isentropic Streams," *Journal of the Aeronautical Sciences*, Vol. 19, No. 10, 1952, pp. 649–676.

[10]Bannink, W. J., Schoones, M. M. J., and Houtman, E. M., "Experimental Study on the Interaction between Linear Plug Nozzle Exhaust Flow and Supersonic External Flow," *Proceedings of the Third European Symposium on Aerothermodynamics for Space Vehicles*, SP-426-1999, ESA–European Space Research and Technology Center, Noordwijk, The Netherlands, 1999, pp. 403–410.

P. Givi
Associate Editor